EVIDENCE FOR SURFACE AND SUBSURFACE ICE INSIDE MICRO COLD-TRAPS ON MERCURY'S NORTH POLE L. Rubanenko[1], E. Mazarico[2], G. A. Neumann[2] and D. A. Paige[1], [1]Department of Earth, Planetary and Space Sciences, UCLA, LA, CA 90095, [2]NASA Goddard Space Flight Center, Greenbelt, MD, USA (liorr@ucla.edu)

Introduction: The small obliquity of Mercury causes topographic depressions located near its poles to cast persistent shadows. Many [1, 9, 15] have shown these permanently shadowed regions (PSRs) may trap water ice for geologic time periods inside cold-traps. More recently, direct evidence for the presence of water ice deposits inside craters was remotely sensed in RADAR [5] and visible imagery [3]. Albedo measurements (reflectence at 1064 nm) obtained by the MErcury Space ENviroment GEochemistry and Ranging Laser Altimeter (MLA) found unusually bright and dark areas next to Mercury's north pole [7]. Using a thermal illumination model, Paige et al. [8] found the bright deposits are correlated with surface cold-traps, and the dark deposits are correlated with subsurface cold-traps. They suggested these anomalous deposits were brought to the surface by comets and were processed by the magnetospheric radiation flux, removing hydrogen and mixing C-N-O-S atoms to form a variety of molecules which will darken with time. Here we use a thermal illumination model to find the link between the cold-trap area fraction of a rough surface and its albedo. Using this link and the measurements obtained by MESSENGER we derive a surface and a subsurface ice distribution map on Mercury's north pole below the MESSENGER spatial resolution, ~ 500 m. We find a large fraction of the polar ice on Mercury resides inside micro cold-traps (of scales $10-100$ m) distributed along the inter-crater terrain.

The Bimodal Albedo Distribution: When we examine the albedo distribution of Mercury's north pole we find it is bimodal with an extended tail (Figure 1). The dark regions have an albedo $< 6\%$ while the bright regions have an albedo $> 25\%$. We use this distribution to model the surface reflectance, which will be explained next. To describe the mean albedo of the surface we use the mean of the higher mode, $\sim 16\%$, and to describe the anomalous dark deposits we use the mean of the lower mode $\sim 4\%$. We consider slopes as bright if their albedo is higher than 25%.

Modeling Rough Surfaces: In the absence of atmospheric erosion, topography on airless bodies can be divided into craters and inter-crater terrain. While craters have a well defined, closed shape (in map view), inter-crater topography is more random in nature. A common method in which this type of topography can be modeled is by using random Gaussian surfaces [2, 6, 14]. Such surfaces are created by modifying the power spectrum of a random field (2D) of normally distributed slopes according to measured parameters such as the Hurst exponent [13] and RMS slope σ_s. Since the Hurst exponent and RMS slope are unknown for Mercury at our scales of interest, we assume values measured on the Moon [10]; surfaces in scales $10-100$ m have an RMS slope $\sigma_s = 10°-15°$. An example for such a surface with $\sigma_s = 15°$ can be seen in Figure 2.

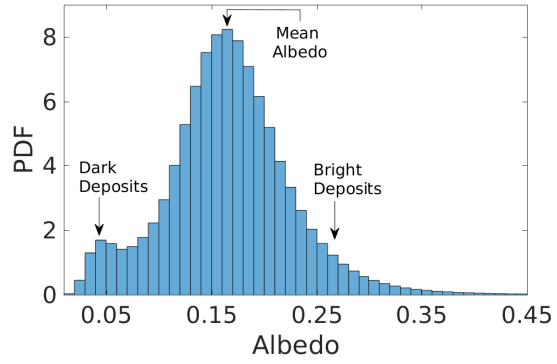

Figure 1: The albedo (reflectance at 1064 nm) distribution of Mercury's north pole between latitudes $75°$ and $84°$. The histogram shows the probability density function (PDF) with a bin width of 0.01.

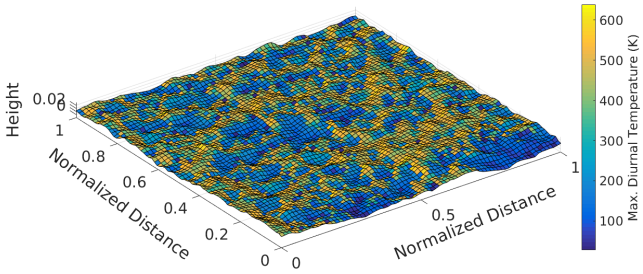

Figure 2: An example for the modeled maximum temperatures on a modeled rough surface with $\sigma_s = 15°$.

Modeling Cold-Traps: We choose to define a cold-trap as an area in which the mass loss rate of water ice < 1 cm Ga^{-1}. This mass loss rate (and thus the stability of cold-traps) is extremely sensitive to changes in temperature. For example, for the mass loss rate we chose, a surface cold-trap must not exceed a maximum temperature of 110K [15]. Subsurface cold-traps are more stable than surface cold-traps due to the diffusion barrier created by the overlaying regolith, and are modeled by considering the dependence of the mass loss rate on depth and temperature [12]. To find the maximum temperature distribution on and below a rough surface, we employ a thermal illumination model accounting for insolation, scattering, thermal emission and conduction into the subsurface in 1D [11]. The thermal parameters we use (conductivity, heat capacity) vary with depth and temperature, but the typical thermal inertia and skin-depth are ~ 25SI and ~ 10 cm. Using the derived maximum temperature distribution, we find the cold-trap area fraction on and below the surface. Next, we link the cold-traps area fraction and the

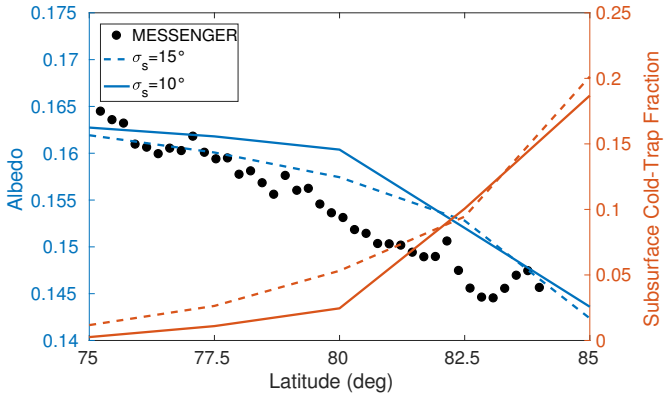

Figure 3: Comparison between the MESSENGER measured mean albedo (over a latitude ring) and the results of the model (LHS y-axis) assuming two roughness values, $\sigma_s = 10°$ and $\sigma_s = 15°$. The RHS y-axis shows the corresponding subsurface cold-trap area fraction.

albedo on rough surfaces.

Linking Cold-Traps and Albedo: To model the surface reflectivity we assign surface cold-traps with an albedo of 25%, subsurface cold-traps with an albedo of 4% and non cold-trapping regolith with an albedo of 16%. The overall surface albedo will simply be the linear combination of the albedo of the slopes composing it [4]. In Figure 3 we show the modeled albedo compared to the latitudinal mean albedo measured by MESSENGER. As we do not account for craters, our modeled albedo slightly deviates from the mean measured albedo. However, our model predicts the 2% decrease in albedo between latitude $75° - 84°$ witnessed by MESSENGER. On the RHS y-axis (red) we show the corresponding area fraction of subsurface cold-traps. We find that in polar latitudes, rough random Gaussian surfaces have a subsurface cold-trap area fraction of up to $\sim 20\%$.

Micro cold-traps on Mercury's north pole: Finally, we employ the correlation we found above and the results of a thermal illumination model at larger scales to create maps of surface and subsurface ice below MESSENGER's spatial resolution. Figure 4 is an example for one of the maps we created, showing the distribution of subsurface ice on Mercury's poles - assuming the roughness in scales of ~ 10 m is $\sigma_s = 10°$. As previously shown [8], we find ice is stable on the permanently shadowed, pole-facing slopes of craters due to their protective closed shape. We find subsurface ice may persist even in areas outside craters, where the maximum temperature distribution is controlled by the small scale roughness and PSR distribution. For a given latitude, the number of permanently shadowed slopes increases when the roughness increases and slopes with surface cold-traps replace slopes with subsurface cold-traps. However, the number of subsurface cold-traps increases as well, and the overall albedo of the

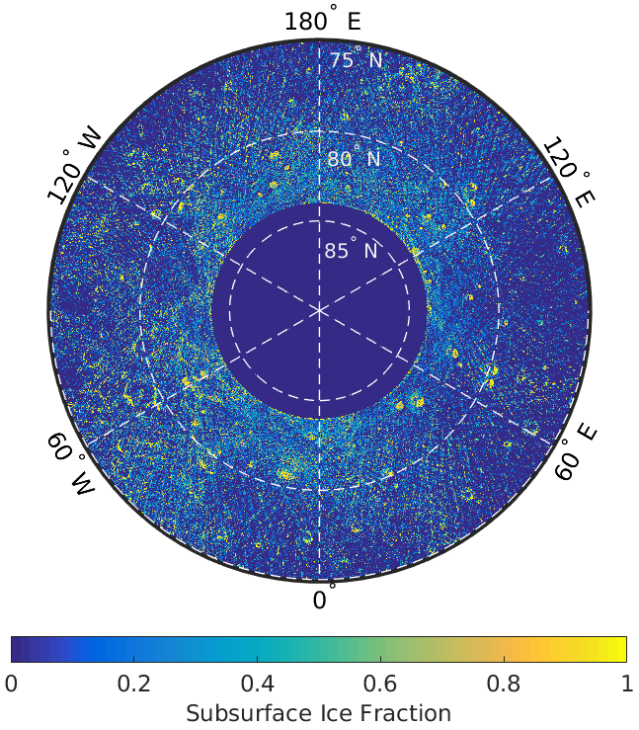

Figure 4: One of the maps produces using our derived link between albedo and ice stability; the distribution of subsurface ice on Mercury's pole in area smaller than the MESSENGER scale, assuming the roughness in scales 10m is $\sigma_s = 10°$.

surface slightly decreases. Assuming Mercury's polar intercrater terrain is a Gaussian random surface with RMS slope $\sigma_s = 10°$, we find it holds $\sim 3\%$ subsurface ice (below dark, weathered regolith) and $\sim 1\%$ surface ice. We conclude a significant amount of the ice on Mercury's north pole is contained inside micro cold-traps created by small-scale rough features. While most of the polar ice is trapped on the permanently shadowed pole-facing slopes of craters, ice within small scale (micro) cold-traps is potentially more accessible and therefore easier to investigate.

References: [1] JR Arnold. *JGR: Solid Earth* 84 (1979), 5659–5668. [2] JL Bandfield et al. *Icarus* 248 (2015), 357–372. [3] NL Chabot et al. *Geology* 42 (2014), 1051–1054. [4] B Hapke. 2012. [5] JK Harmon et al. *Icarus* 149 (2001), 1–15. [6] JSV Lagerros. *Astronomy and Astrophysics* 325 (1997), 1226–1236. [7] GA Neumann et al. *Science* 339 (2013), 296–300. [8] DA Paige et al. *Science* 339 (2013), 300–303. [9] DA Paige et al. *Science* 258 (1992), 643–646. [10] MA Rosenburg et al. *JGR: Planets (1991-2012)* 116 (2011). [11] L Rubanenko et al. *Lunar and Planetary Science Conference*. Vol. 47. 2016, 1650. [12] N Schorghofer et al. *JGR: Planets (1991-2012)* 112 (2007). [13] MR Schroeder. 2012. [14] BG Smith. *JGR* 72 (1967), 4059–4067. [15] K Watson et al. *JGR* 66 (1961), 3033–3045.